Removal of dyes from aqueous solution using Bis [Hg (2-Apt)]-modified Fe$_3$O$_4$ magnetic nanoparticles

Aveen Faidhalla Jalal*, Nabil Adil Fakhre

Department of Chemistry, College of Education, Salahaddin University-Erbil, Kurdistan Region, Iraq, Tel. +9647504552485; emails: aveen.jalal@su.edu.krd/faidhallajalalaveen@gmail.com (A.F. Jalal), nadil.fakhre@su.due.krd (N.A. Fakhre)

ABSTRACT

A novel adsorbent Bis [Hg (2-Apt)]-Fe$_3$O$_4$ nanoparticle was successfully synthesized and resultant adsorbent characterized through Fourier-transform infrared spectroscopy, scanning electron microscopy, energy-dispersive X-ray spectroscopy, X-ray diffraction, and transmission electron microscopy analyses. The adsorption capacity of Bis [Hg (2-Apt)]-Fe$_3$O$_4$ towards Brilliant green (BG) and Methylene blue dyes was examined. Effects of pH, adsorbent dosage, and dye concentration for the adsorption process were investigated. The removal efficiency in optimal conditions (pH = 5, dye concentration = 20 mg/L, contact time 120 and 70 min and adsorbent dose = 0.02 g/10 mL and 0.015 g/10 mL) for the Methylene blue and BG was obtained 97.55% and 100% respectively. Moreover, adsorption experiments were employed to evaluate adsorption kinetic, isotherm, Gibbs free energy, and reusability. Isotherm experiments indicated that the Langmuir model is the best mathematical models for fitting. It can be concluded Bis [Hg (2-Apt)]-Fe$_3$O$_4$ nanoparticles are considered promising cationic dye adsorbents with excellent removal efficiency, regeneration, and reuse ability.

Keywords: Nanocomposites; Bis-(2-amino phenyl thio) mercury; Cationic dye; Adsorption; Isotherm; Kinetics

1. Introduction

The development of industries especially textile and dyestuff has caused a high quantity of wastewater content dye pollutants in the environment [1]. Organic compounds (e.g., dyes), heavy metals, radionuclides, and pathogens are the main pollutants in industrial effluents [2,3]. Dyes are the main environmental concern due to acute threats to ecological and human health. The molecular structure of dyes includes auxochromes, OH, NH$_2$, NHR, and NR$_2$, with chromophores being NO$_2$, NO, and N = N. Chromophores are responsible for giving dyes color, whereas auxochromes increase the intensity of dyes. Meanwhile, cationic dyes are more hazardous than anionic dyes due to

chemical characteristics, mutagenicity, carcinogenicity, and poisonous [4–6]. Methylene blue (MB) is the cationic dye with the chemical formulation C$_{16}$H$_{18}$N$_3$SCl and a molecular weight of 319.65 g/mol. Exposure to MB causes serious human health problems, including nausea, vomiting, jaundice, elevated heart rate, excessive perspiration, mental disorientation, cyanosis, and quadriplegia [7]. Brilliant green (BG) is a cationic dye widely used in biological staining, dermatological agents, veterinary medicine, and poultry feed to inhibit the propagation of mold, intestinal parasites, and fungus. BG is extremely toxic for humans (e.g., harmful to skin, eyes, digestive system, and lungs) and the environment [8]. BG due to the existence of C,S, and N elements in the molecular structure can release carbon

* Corresponding author.

dioxide, sulfur oxides, and nitrogen oxides pollutants into the environment during the degradation process (Fig. S1) [9].

The adverse effects of MB and BG on humans and the ecology suggest the importance of removing them from aquatic environments through the design and development of dye treatment materials/technologies.

Studies show that various physical, chemical, and biological methods including advanced oxidation process, electrochemical process, membrane technology, activated sludge and absorption have been used to treat dye-containing wastewater. Although these methods have been effective in removing organic pollutants, they suffer from many restrictions such as high energy consumption, the release of aromatic amines, high-cost operation, non-complete pollutant degradation, and generating harmful waste products.

Adsorption is a promising approach for pollutant removal due to its ease to use, low operating cost, simplicity of design, non-susceptibility to hazardous contaminants, reusability, high removal effectiveness, and wide availability of adsorbent kinds [9]. MB and BG due to high chemical stability and low biodegradability (the existence of complex aromatics in the molecular structure), need to use effective techniques with high capabilities in dye removal without causing secondary pollution or producing highly toxic by-products.

Magnetic nanoparticles (MNPs) gaining much attention as an alternative adsorbent for water treatment due to their inexpensive and easy manufacturing, fast adsorption kinetics, high-specific surface area, easy separation by the external magnetic field, and reusability [7]. The present study aims to continue to look at the benefits of both green and nanoparticle-based materials. For the first time, aqueous plant extract of *Gundelia tournefortii* L (Family name, Asteraceae and Local name, Kangir) was used as a rapid and green technique for the generation of Fe_3O_4 NPs, then the Bis [Hg (2-Apt)]-Fe_3O_4 NPs were synthesized as a novel separable sorbent to enhance the removal of MB and BG dyes. The Fe_3O_4 NPs and Bis [Hg (2-Apt)]-Fe_3O_4 NPs were characterized using X-ray diffraction (XRD), Fourier-transform infrared spectroscopy (FTIR), scanning electron microscopy (SEM), transmission electron microscopy (TEM), and vibrating sample magnetometer (VSM) techniques. Also, the effect of operational parameters including contact time, initial dye concentration, pH, adsorbent dosage, temperature, as well as adsorption capacity, selective adsorption kinetic, sorption isotherm, restoration, and recycling of the materials were studied.

2. Material and methods

2.1. Reagents

Ethanol (C_2H_5OH), ferric chloride hexahydrate ($FeCl_3 \cdot 6H_2O$), Iron(II) sulfate heptahydrate ($FeSO_4 \cdot 7H_2O$), mercuric acetate, and 2-aminothiophenol were purchased from Sigma Aldrich (St. Louis, MO, USA). Brilliant green (BG), Methylene blue (MB), H_2SO_4 (>99.0%), HCl (35%–37%), and sodium hydroxide NaOH (93%) were purchased from Merck Co., (Darmstadt, Germany). All other chemicals were of analytical grade and used as received without any further purification.

2.2. Preparation of plant extract

The plant *Gundelia tournefortii* L (family name, Asteraceae and local name, Kangir), was collected from the local mountain of Kurdistan Region-Iraq, washed several times with tap water and distilled water, shade dried, chopped up into tiny bits, and powdered. The plant extract was produced with some modifications, 5.0 g of the powdered plant was transferred into a conical flask containing 100 mL of deionized water (DW). The obtained extract was heated at 60°C for 15 min, cooled under ambient conditions and filtered using a filter paper Whatman No.1. Finally, the light brown solution was maintained and placed at 4°C [11,12].

2.3. Synthesis of Fe_3O_4 nanoparticles

Iron oxide nanoparticle was synthesized as follow: 20 mL of $FeCl_3 \cdot 6H_2O$ solution and 20 mL of $FeSO_4 \cdot 7H_2O$ (1:2 molar ratios) were added into 100 mL of plant extract. The mixture was continuously stirred and sodium hydroxide (1.0 M) was added dropwise to the solution mixture until the pH of the solution was raised to 11. The solution was agitated for 1.0 h in order to more homogeneity of mixture and Fe_3O_4-NPs were subsequently collected by an external magnetic field. The obtained Fe_3O_4-NPs were washed with deionized water several times and dried for 24 h in an oven (70°C).

2.4. Synthesis of bis-(2-amino phenyl thio) mercury [Hg (2-Apt)]

According to Ameen et al. [13], bis-(2-amino phenyl thio) mercury [Hg (2-apt)] was synthesized. Briefly, 5.0 g of 2-aminothiophenol (40 mmol) was mixed with 6.0 g of mercuric acetate (20 mmol,) in 25 mL of methanol. The mixture agitated at room temperature for 5.0 h until the green particles developed. The obtained product was separated by filtration, dried in the air, and recrystallized from ethanol.

2.5. Synthesis Bis [Hg (2-Apt)]-Fe_3O_4 NPs

Bis [Hg (2-Apt)]-Fe_3O_4 NPs were synthesized based on a technique described in the previous literature [14]. Firstly, 0.5 g of Fe_3O_4 nanoparticles, and 0.25 g of [Hg (2-Apt)] were transferred in a 25 mL beaker containing water: ethanol (2:1 v/v), and then a uniform suspension was obtained via ultrasound water bath (5.0 h). Finally, the Bis [Hg (2-Apt)]-Fe_3O_4 NPs were separated from the reaction medium by an external magnetic field, rinsed many times with deionized water and dried in the oven for further subsequent experiments.

2.6. Characterization of Fe_3O_4 Nps and Bis [Hg (2-Apt)]-Fe_3O_4 NPs

The PANalytical X'Pert PRO X-ray diffractometer (XRD) was used to evaluate the crystal structure and purity of the adsorbents using monochromatic graphite copper radiation (Cu Ka, λ = 1.54 A°) at 40 kV, 40 mA, and 25°C. Fourier transform infrared (FT-IR) spectroscopy (SHIMADZU IR AFFINITY-I FTIR spectrophotometer) was employed to study the presence of the biomolecules

which are responsible for the synthesis of Fe_3O_4 NPs and Bis [Hg (2-Apt)]-Fe_3O_4 NPs. For this aim, dried samples were ground with potassium bromide (KBr) to produce a pellet, and examined in a wavelength range of 400–4000 cm^{-1}. The surface morphology, textural structure, and elemental constituents of samples were investigated by SEM and energy-dispersive X-ray spectroscopy (EDX) using Merlin Compact 6073 scanning electron microscope (Carl Zeiss, Germany). The size and morphology of the adsorbents were observed using the TEM (FEI TECNAI G2 F20). The magnetic properties of the nanoparticles in the applied magnetic field were measured at room temperature with a vibrating sample magnetometer (VSM) made by Daghigh Kavir Corporation. The residual concentration of MB and BG dyes was determined by Shimadzu UV-visible spectrophotometer (UV-1800, Japan) at 664 and 618 nm respectively. Fig. 1 shows the UV-Vis spectra of the solution before and after adsorption.

2.7. Batch adsorption procedure

Batch experiments were conducted to evaluate the effect of operational parameters including adsorbent dosage (10–35 g/L), pH (2–12), initial dye concentration: 20 mg/L; pH: 5; contact time: 2 h and adsorbent dosage 25 g.
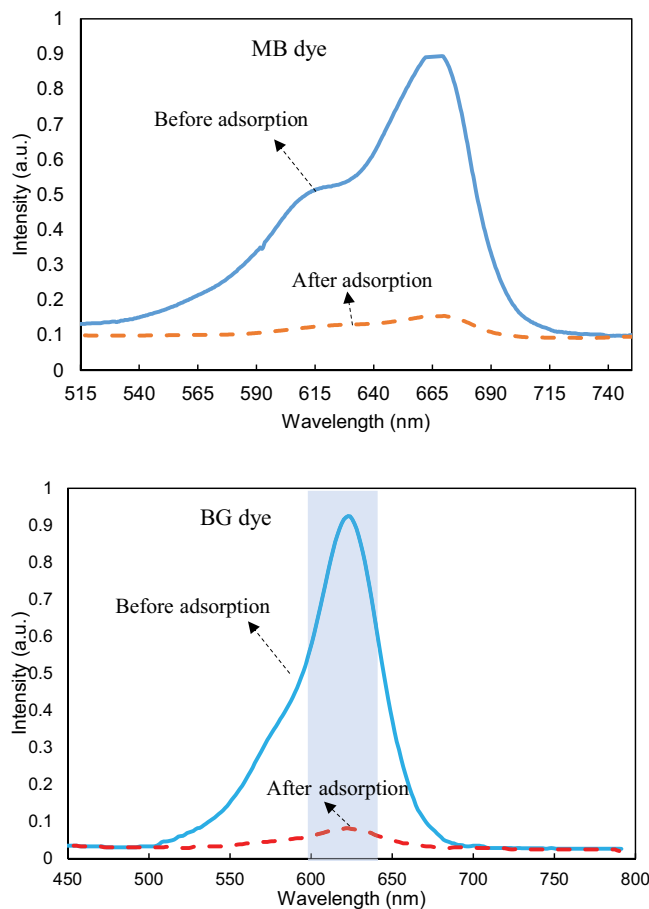

Fig. 1. UV-Vis spectra of the solution before and after adsorption of BG and MB dyes

20 mg of Bis [Hg (2-Apt)]-Fe_3O_4 NPs and 10 mL dye solution at the certain concentration were added to a 12 mL test tube. Except for the adsorption kinetics experiment, the tube was kept in a water bath oscillator thermostat for 24 h at 180 rpm. The desired pH was adjusted with few droplets of NaOH (1N) and HCl (1N) solutions. The sampling was carried out in a certain interval time and the residual concentration of MB and BG dyes was determined using a Spectrophotometer at 664 nm and 618 nm respectively. The quantity of MB and BG adsorbed onto the adsorbent and removal efficiency were computed according to Eqs. (1) and (2):

$$q_e = \frac{\left[(C_i - C_e)V\right]}{W} \tag{1}$$

$$R\% = \left[\frac{(C_i - C_e)}{C_i}\right] \times 100 \tag{2}$$

where q_e (mg/g) is equilibrium capacity of a sorbent, V (L) is a volume of solution, W (g) is mass of sorbent, C_i and C_e were initial and equilibrium concentration (mg/L) of MB and BG, respectively and R is the removal percent of dyes.

Isotherms are mathematical equations that describe the adsorption behavior of a certain adsorbent–adsorbate combination. Langmuir, Freundlich, and Temkin models are used to fit the obtained data from the adsorption process [13,14]. The Langmuir model is the most frequently used model in the adsorption process [Eq. (3)].

$$\frac{C_e}{q_e} = \frac{1}{q_m K_L} + \frac{C_e}{q_m} \tag{3}$$

where C_e (mg/g) denotes the adsorbate concentration at equilibrium. K_L is a Langmuir constant related to adsorption capacity (mg/g) that can be connected with variations in the appropriate area and porosity of the adsorbent, implying that adsorption capacity will be larger if the surface area and volume are large. The separation factor R_L is a dimensionless constant that expresses in Eq. (4), the essential characteristics of the Langmuir isotherm.

$$R_L = \frac{1}{1 + K_L C_e} \tag{4}$$

where R_L value shows the adsorption nature to be either unfavorable ($R_L > 1$), linear ($R_L = 1$), favorable ($0 < R_L < 1$) or irreversible ($R_L = 0$).

Freundlich describes the non-ideal and reversible adsorption with the formation of multilayers and with a non-uniform distribution of adsorption heat and affinities over the heterogeneous surface. The Temkin isotherm evaluates the adsorbent–adsorbate interaction without considering the amount of adsorbate concentration. The linear form of Freundlich and Temkin isotherms are depicted in Eqs. (5) and (6) respectively.

$$\log q_e = \log K_F + \frac{1}{n}\log C_e \tag{5}$$

$$q_e = K_T + 2.303 b_T \log C_e \tag{6}$$

where $1/n$ indicates adsorption capacity, K_F represents adsorption capacity (L/mg). The slope range between 0 and 1 indicates the intensity of absorption or the heterogeneity of the surface. When the value of this parameter tends to 0, it means that the surface is more heterogeneous. Moreover, the $1/n < 1$ and >1 indicate chemical and cooperative adsorption respectively.

The Temkin constant (b_T) is related to the heat of sorption (J/mol) and the Temkin isotherm constant (K_T) (L/g).

Thermodynamic parameters such as a change in Gibbs free energy ($\Delta G°$), an enthalpy variation ($\Delta H°$), and entropy variation ($\Delta S°$) were computed using Eqs. (7)–(9).

$$K_d = \frac{q_e}{C_e} \tag{7}$$

$$\ln K_d = \frac{\Delta S°}{R} - \frac{\Delta H°}{RT} \tag{8}$$

$$\Delta G° = -RT \ln K_d \tag{9}$$

where T is the absolute temperature (K); R is the universal gas constant (8.314 J/mol·K); enthalpy ($\Delta H°$), and entropy ($\Delta S°$) changes can be determined through intercept of the line obtained using plotting $\ln K_d$ vs. $1/T$. K_d is the adsorption distribution constant derived using q_e/C_e and q_e (mg/g) [15].

Kinetics adsorption of dyes were evaluated using quasi-first-order and quasi-second-order. The linear form of quasi-second-order and quasi-second-order are illustrated in the following equations:

$$\log(q_e - q_t) = \log q_e - \frac{k_1 t}{2.303} \tag{10}$$

$$\frac{t}{q_t} = \frac{1}{q_e} + \frac{1}{k_2 q_e^2} \tag{11}$$

The k_1 (min^{-1}) is the rate constant and k_2 (g/mg·min) rate constant at the equilibrium for the quasi-second-order and quasi-second-order kinetic models, respectively. The values of k_1 and k_2 were determined through intercept and the slope of the plot of $\log(q_e-q_t)$ vs. t and t/q_t vs. t, respectively.

3. Results and discussion

3.1. Characterization

3.1.1. Fourier-transform infrared spectroscopy

Fig. 2 shows the FTIR analysis of different adsorbents. The peak at 3,409 cm^{-1} is related to OH stretching vibration in O–H groups. The absorption spectrum at 1,637 cm^{-1} corresponds to the asymmetric and symmetric C=O bending vibrations. The peaks at 500–700 cm^{-1} are due to the stretching vibration of Fe–O bonds [16]. Ameen BM et al. have reported [13], the infrared spectrum of the free Bis [Hg (2-Apt)] compound is located in the range of

(3,311–3,238) cm^{-1} peaks, which are corresponding to v (NH) of NH$_2$ amine functional groups. The weak bands in the range of 3,012–3,055 cm^{-1} are assigned to v (C–H) aromatic ring. A sharp band absorption at 1,597 cm^{-1} in the spectrum of Bis [Hg (2-Apt)] compound is due to v (C–N) band. The strong band at 750 cm^{-1} is ascribed to (C–S). Results indicate a similar pattern for final adsorbent, which suggested the Bis [Hg (2-Apt)] was successfully grafted onto Fe$_3$O$_4$ MNPs.

3.1.2. Scanning electron microscopy

Figs. 3a–d show the morphology of the sorbent before and after cationic dye adsorption. Pure Fe$_3$O$_4$ was prepared to compare the surface structure of Bis [Hg (2-Apt)]-Fe$_3$O$_4$. Fig. 3a illustrates the surface structure of Fe$_3$O$_4$ which is an aggregated and cage-like structure. After coating Bis [Hg (2-Apt)] on Fe$_3$O$_4$, a folding structure was observed due to surface smooth Bis [Hg (2-Apt)] Fig. 3b. Fig. 3c and d show the morphological features of adsorbent for the adsorption of both cationic dyes. As can be observed the dyes adsorbed have caused the adsorbent surface to be smoother. Moreover, more particles are existing on the surface of Bis [Hg (2-Apt)]-Fe$_3$O$_4$ indicating dye molecules as well as iron oxide particles.

3.1.3. Transmission electron microscopy

Figs. 4a–d illustrate the form and size distribution of the nanoparticle using TEM imaging. Results show the cubic and spherical nanoparticles with an average diameter of 29.9 nm (Fig. 4a and c). Results confirm the particle size calculated using Scherer's equation closely matches the TEM data. Also, the nanoparticles have jumbled together which is called "nanoaggregates". Fig. 4b and d show that the synthesized Bis [Hg (2-Apt)]-Fe$_3$O$_4$ NPs is very fine and their cluster shows that Bis [Hg (2-Apt)] is fully incorporated in Fe$_3$O$_4$ particles.

3.1.4. Energy-dispersive X-ray spectroscopy

The EDX analysis indicates the presence of elements in the composition. Fig. 4a–d show EDX mapping of the Fe$_3$O$_4$
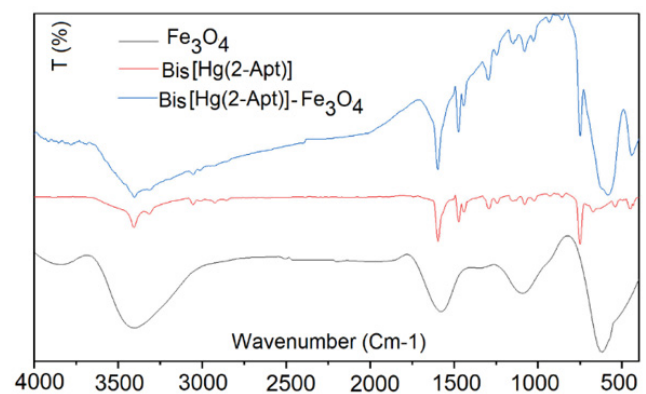
Fig. 2. FTIR spectra of Fe$_3$O$_4$ nanoparticles, Bis [Hg (2-Apt)] and Bis [Hg (2-Apt)]-Fe$_3$O$_4$ nanoparticles.
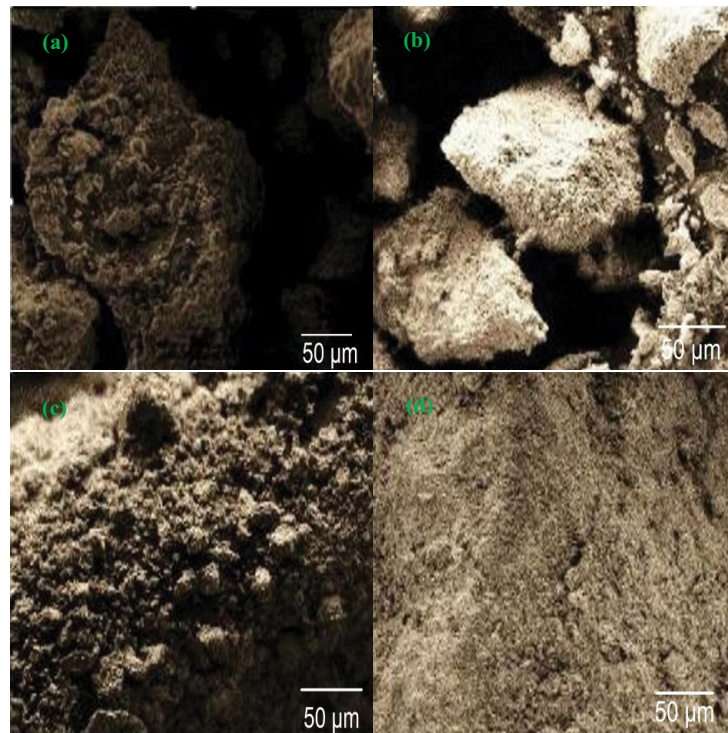
Fig. 3. Microphotograph obtained by SEM of the (a) Fe_3O_4 nanoparticles, (b) Bis [Hg (2-Apt)]-Fe_3O_4 nanoparticles, (c) Bis [Hg (2-Apt)]-Fe_3O_4 nanoparticles after adsorption of MB, and (d) Bis [Hg (2-Apt)]-Fe_3O_4 nanoparticles after adsorption of BG.
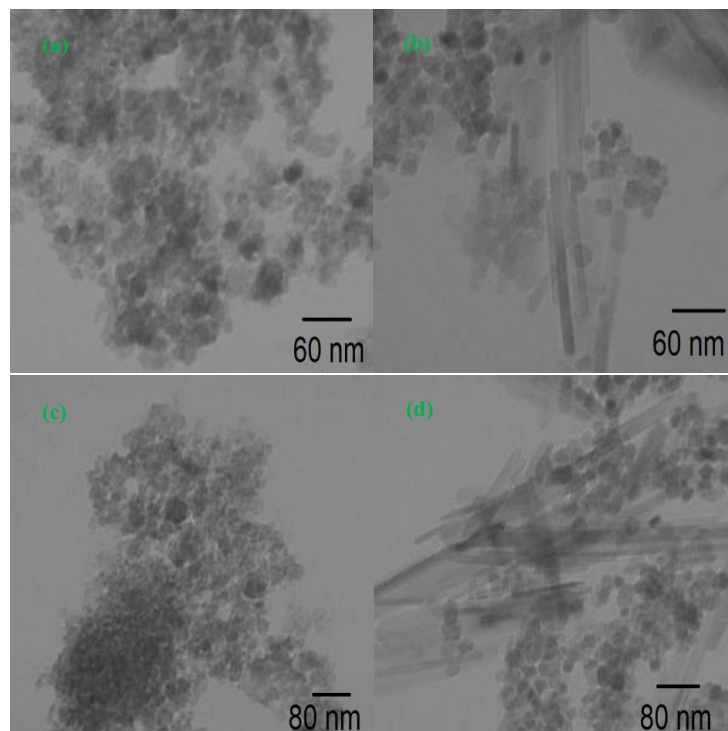

Fig. 4. TEM image of the (a,c) iron oxide nanoparticles and (b,d) Bis [Hg (2-Apt)]-Fe_3O_4 NPs.

and Bis [Hg (2-Apt)]-Fe_3O_4, after MB and BG adsorption. Fig. S2a illustrates O and Fe. The presence of a high amount of iron ions inside of the nanoparticles induces the production of magnetite nanoparticles using the plant [17]. Fig. S2b indicates new elements such as C, N, S, and Hg suggested the Bis [Hg (2-Apt)] successfully grafted on Fe_3O_4 nanoparticles. Fig. S2c and d demonstrated the EDX analysis of both MB and BG after sorption on sorbent respectively.

3.1.5. X-ray diffraction

Fig. 5 shows the crystallographic structure of the magnetic nanoparticles synthesized by *Gundelia tournefortii* L extract. The peaks reflect amorphous structures (220), (104), (311), (222), (400), (422), (511), (410) and (533) of iron oxide. Additionally the rhombohedral structure of iron oxide may be indexed to all of the reflection peaks (JCPDS NO. 89-8104). Similar to iron oxide nanoparticles, these studies describe a crystalline form [18,19]. The Debye–Scherrer formula showed average particle size is 29.6 nm. The XRD analysis indicated that the crystallite size of the Fe_3O_4-NPs generated ranged between (11.7–69.3) nm which was matched with the TEM result [20]. The XRD pattern of Bis [Hg (2-Apt)]-Fe_3O_4 magnetic nanoparticles showed feature peaks nearly equal to the normal Fe_3O_4 XRD patterns with a medium estimated diameter of 31.45 nm, which indicates that the Fe_3O_4 type is not changed. The diffraction peaks were indexed to the (012), (120), (220), (104), (130), (311), (222), (400), (422), (116) and (511) planes of Bis [Hg (2-Apt)]-Fe_3O_4 cubic phase. This result suggested that coating of Bis [Hg (2-Apt)] on iron oxide does not degrade the core magnetite. Although a number of new peaks have appeared which are assigned to the other iron oxide like Fe_2O_3 (012), (104) and (116) and FeOOH (120), (130). Yew et al. have reported that Fe_2O_3 could be formed in green synthesis of Fe_3O_4 using seaweed (kappaphycus alvarezii) extract [20]. The magnetic sizes of Fe_3O_4 and PVA-Fe_3O_4 were extremely similar to the findings of the TEM investigation.

3.1.6. VSM

VSM was employed to evaluate the magnetic properties of the adsorbent. Briefly, magnetometry is used to quantify the nanocomposite's generated magnetic properties in the field of 20,000 to −20,000, which is known as the magneto-resistance (MR) effect. Fig. 6 shows the VSM analysis of the Fe_3O_4 and Bis [Hg (2-Apt)]-Fe_3O_4. A soft magnetic property characterized by high saturation magnetization values o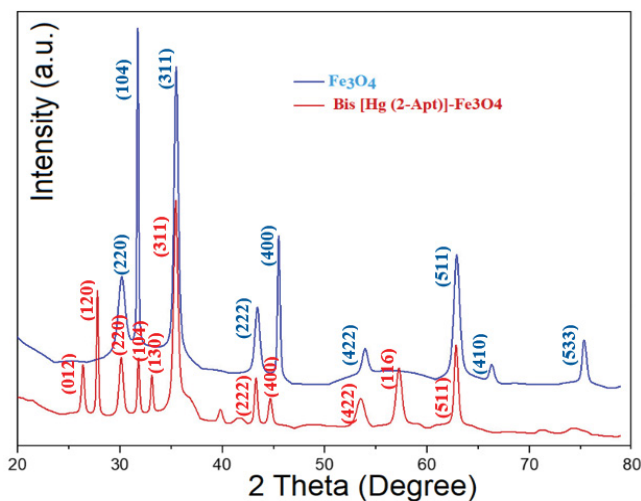f 48.6 emu/g is shown in the image which suggested the superparamagnetic nature of the nanoparticle due to the smaller size of Fe_2O_3 particles [21,22]. The result indicated the saturation magnetization value for Bis [Hg (2-Apt)]-Fe_3O_4 nanoparticles is 36.4 emu/g. The decrease in mass saturation magnetization may be due to the non-magnetic Bis [Hg (2-Apt)] property to the total mass of particles [14].

3.2. Effect of adsorption conditions

3.2.1. Adsorption time effect and kinetic study

Fig. 7a shows the impact of contact time on the MB and BG removal. The result indicated in the early minutes the removal efficiency of MB reached 61.58%. With increasing the contact time (120 min), the removal efficiency raised rapidly to 97.28% and then constant. The results revealed the condition is slightly different for BG removal. As Fig. 7a has shown the removal efficiency increased rapidly (98.1%) in the first 10 min. This is due to the high number of specialized binding sites for BG dye molecules on the adsorbent surface. Then removal efficiency increased slightly reaching a maximum value (100%) at 70 min suggesting dye molecules have occupied all active binding sites on the adsorbent surface during the adsorption process. Thus, 70 min was selected for further conduction of experiments.

Pseudo-first-order and pseudo-second-order kinetic models were employed to fit the data (Figs. 7b-e). Table 1 provides the fitting parameters for the kinetic models. The correlation coefficient was used to evaluate the quality of fit between the computed ($q_{e,\text{cal}}$) and experimental data ($q_{e,\text{exp}}$).

Results indicate a poor linear regression coefficient (R^2) for pseudo-first-order than pseudo-second-order for both MB and BG dyes (Table 1). Furthermore, the $q_{e,\text{exp}}$ value derived by pseudo-second-order was consistent with the $q_{e,\text{cal}}$ value. This implies that the pseudo-second-order kinetic model well describes the adsorption of both dyes by the adsorbent.

3.3. Effect of pH on adsorption

pH through the effect on the adsorbent and adsorbate properties plays a significant role in the adsorption

Fig. 5. X-ray diffraction patterns of magnetic nanoparticles Fe_3O_4 and Bis [Hg (2-Apt)]-Fe_3O_4
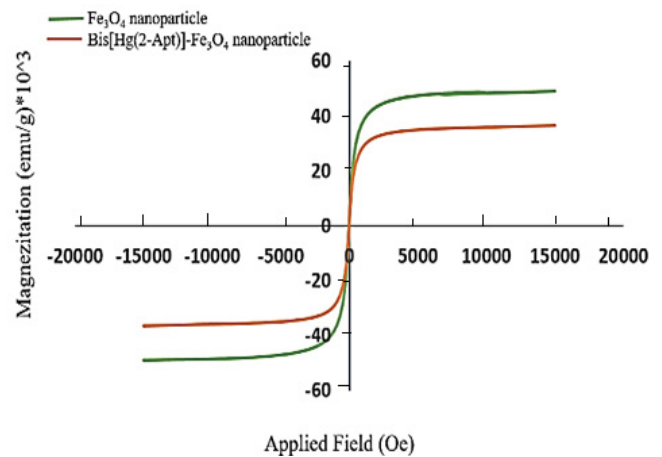

Fig. 6. Room temperature magnetization curve for Fe_3O_4 and Bis [Hg (2-Apt)] nanoparticles.
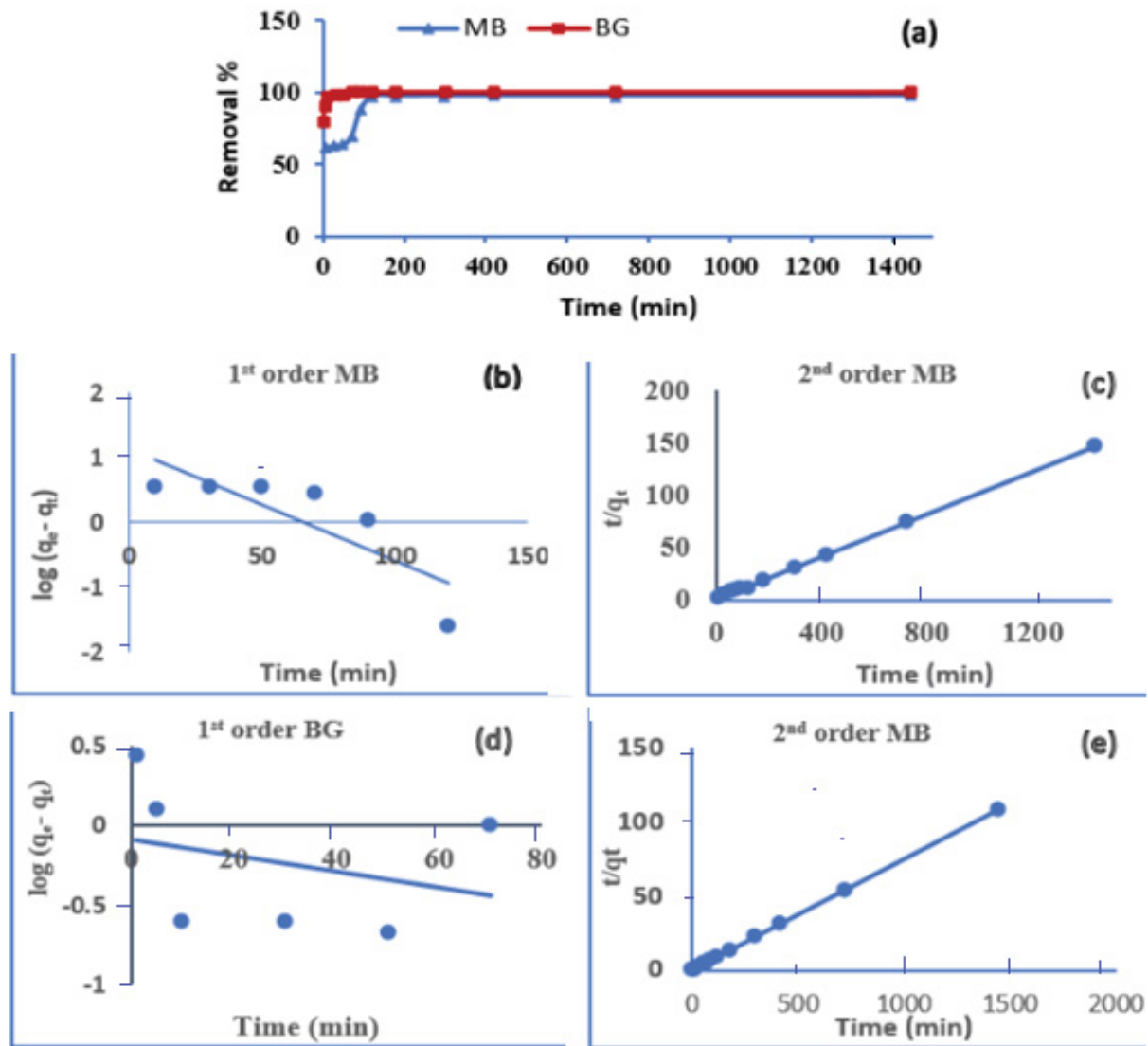
Fig. 7. (a) Adsorption time impact of MB and BG removal, (b) MB pseudo-first-order kinetics plots, (c) MB pseudo-second-order kinetics plots, (d) BG pseudo-first-order kinetics plots, and (e) BG pseudo-second-order kinetics plots.

Table 1
Kinetic characteristics for the adsorption of MB and BG onto Bis [Hg (2-Apt)]-Fe$_3$O$_4$ nanoparticles

Dye	Pseudo-first-order			Pseudo-second-order		
	R^2	q_{cal} (mg/g)	$K \times 10^{-2}$ (min^{-1})	R^2	q_{cal} (mg/g)	$K \times 10^{-3}$
MB	0.6857	9.89	7.83	0.9995	9.73	14.17
BG	0.0943	13.33	39.8	1.0	13.33	0.8292

process. Hence, it affects the dye stability and charge of the adsorbate functional group, facilitating dye removal via selective sorbent [23].

Fig. 8 shows the removal efficiency of MB and BG increased from 89.93% to 98.99% and 90.6% to 100% with a change in pH from 2.0 to 5.0 respectively. While, at pH = 12.0, the removal efficiency of MB dropped to 41.49%, and the amount of BG removal remained constant. Similar findings have been reported in other publications for MB [24,25] and BG [26].

3.4. Concentration of initial dyes effect

Fig. 9 shows the effect of initial dye concentrations (5–50 mg/L) on the removal efficiency of MB and BG by Bis [Hg (2-Apt)]-Fe$_3$O$_4$ nanoparticles. Results indicated
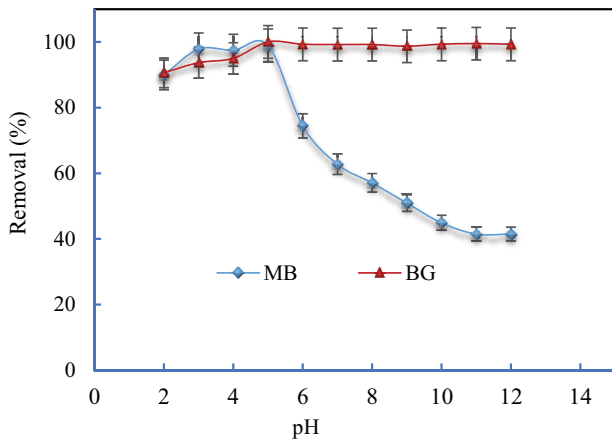
Fig. 8. Effect of pH on MB dye and BG dye removal (initial dye concentration: 5 mg/L; adsorbent dosage 35 g/L; contact time: 24 h).
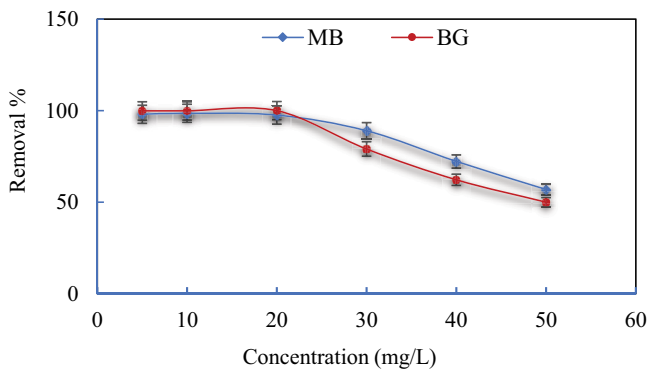

Fig. 9. Effect concentrations of MB and BG on removal efficiency (pH: 2; adsorbent dosage 35 g/L; contact time: 24 h).

removal efficiency is dropped with increasing the initial dye concentration. Results revealed with increasing the dye concentration from 5 to 20 mg/L, the removal efficiency of MB and BG increases up to 97.5% and 100%, respectively. This suggested the adequate number of active sites occupied by dye molecules at low dye concentrations. While increasing the initial concentration of dye from 20 to 50 mg/L, the removal efficiency of MB and BG decreased from 97.55% to 56.92% and 100% to 50%, respectively. This phenomenon is due to the fact that the number of active sites of absorbent is constant, therefore, with the increase in dye concentration (>20 mg/L), the active sites are saturated and the efficiency decreases [5,27]. Results suggested the optimal MB and BG concentration is 20 mg/L.

3.5. Effect of adsorbent dose

The effect of the adsorbent dose is investigated in order to evaluate the ability of the minimum dosage of adsorbent for dye adsorption. For this aim, different adsorbent dosages (10, 15, 20, 25, 30 and 35 mg) were used to remove the MB and BG (20 mg/L). Fig. 10 shows that with increasing adsorbent dosage from 10 to 35 mg, the removal efficiency increased significantly from 78.98% to 97.85% for MB and
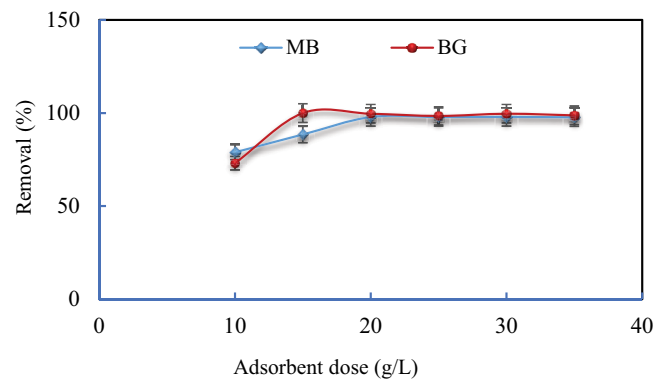

Fig. 10. Effect of adsorbent dose on removal dye (initial dye concentration: 5 mg/L; pH: 2; contact time: 24 h).

73.05% to 99.61% for BG. The results indicated the adsorption process increases rapidly with increasing of adsorbent dose at first and then reached equilibrium at optimum dosage. This is due to the development of the number of active sites accessible at the adsorbent surface. However, further dye adsorption with increasing the adsorbent mass does not occur due to overlapping of sorption sites caused by overcrowding of active sites [8,28]. According to the results, the 20 mg and 15 mg dosages were considered optimal dosages for the removal of MB and BG respectively.

3.6. Effect of temperature

The effect of temperature (10°C–45°C) was studied as an indicator of the adsorption nature in order to determine whether the adsorption process is exothermic or endothermic. The results showed with changes in the temperature from 10°C to 35°C, the removal efficiency of MB and BG increased from 78.77% to 97.15% and 56.35% to 99.17%, respectively suggesting the process is an endothermic process (Fig. 11). The increase in removal efficiency with raising the temperature is due to increasing the mobility of the MB and BG molecules and an increase in the number of active sites. As well as, high temperature provides enough energy for dye molecules more engage with adsorption sites on the Biscuit's surface [Hg (2-Apt)]-nanoparticles of Fe_3O_4 [29]. Furthermore, increasing the temperature causes the internal structure of the adsorbent to expand as a result more dye molecules will be adsorbed. Results indicated the removal efficiency is decreased for higher temperatures (>35°C). High temperature may induce desorption behavior during the adsorption process for the violent molecular motion at temperatures over 30°C, as a result decreasing the removal efficiency [30]. In this work, 30°C was selected as the optimum temperature for further experiments.

Thermodynamic analysis of the adsorption process is generally useful for determining the process's spontaneity, unpredictability, endothermicity, or exothermicity. The effect of temperature on the MB and BG dye adsorption onto Bis [Hg (2-Apt)]-Fe_3O_4 sorbent was investigated using thermodynamics. Gibb's free energy (DG), entropy (DS), and enthalpy (DH) were computed using linear plots of ln K_d vs. 1/T, the values of DS and DH were calculated

from intercept and slope, respectively [2]. Table 2 shows the values of thermodynamic parameters Results showed DG value is negative for both dyes at the studied temperature ranges suggesting that the adsorption process is spontaneous. Moreover, the DH value for MB and BG was obtained at 67.81 and 140.54 kJ/mol, respectively. The positive value of DH suggests that cationic dye adsorption is endothermic. As well as, the positive values of DS

for MB (240.25 J/mol·K) and BG (487.6 J/mol·K) suggest a strong affinity of dye molecules towards the adsorbent surface. The positive values of DS and DH indicate the chemisorption of dye molecules by adsorbent [26,31].

3.7. Adsorption isotherms models study

Adsorption isotherms describe how the adsorbate interacts with the adsorbent. In addition, they also present the absorption capacity of the adsorbent [26]. Langmuir, Freundlich, and Temkin were used to fit the obtained data. The components and coefficients of correlation for Langmuir, Freundlich, and Temkin adsorption isotherm models onto Bis [Hg (2-Apt)]-Fe$_3$O$_4$ nanoparticles are presented in Table 3. Fig. 12 illustrates the linear regression of the MB and BG adsorption isotherm models onto Bis [Hg (2-Apt)]-Fe$_3$O$_4$ nanoparticles. Results indicated Langmuir isotherm has the greatest correlation coefficient (R^2), indicating that the adsorption process was matched to the Langmuir model and monolayer adsorption. K_L and R^2 parameters explain the strong adsorption capacity. K_L and R^2 values for Bis [Hg (2-Apt)]-Fe$_3$O$_4$ and Fe$_3$O$_4$ were obtained 3.14 L/mg, 7.29 L/mg, 0.9998, and 0.9998, for MB and BG respectively. These results indicate a great affinity between adsorbate and adsorbent. The R_L values of the MB and BG dyes were obtained (0.0063–0.0598) and (0.0027–0.0267), respectively, indicating that the adsorption process is favorable ($0 > R_L > 1$). The maximum monolayer adsorption capacity (q_m) of MB and BG dye were obtained 14.6 and 16.7 mg/g, respectively. It was higher than other reported adsorbents (Table 3).

3.8. Desorption and reusability

The reusing ability of an adsorbent is essential for cost-effective and environmentally sustainable water treatment. The main advantage of nanoparticles containing Fe$_3$O$_4$ is their easy separation by an external magnet which facilitates the reusability of the adsorbent. Desorption study is employed to interpret the mechanism and recovery of the adsorbate and adsorbent. Desorption efficiency of Bis [Hg (2-Apt)]-Fe$_3$O$_4$ nanoparticles was conducted using a desorbing solution such as ethanol, methanol, hydrochloric acid (0.1 and 1.0 N), sodium hydroxide (0.1 and 1.0 N), and distilled
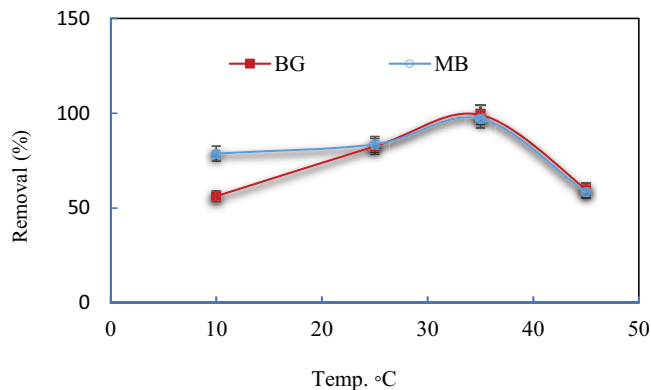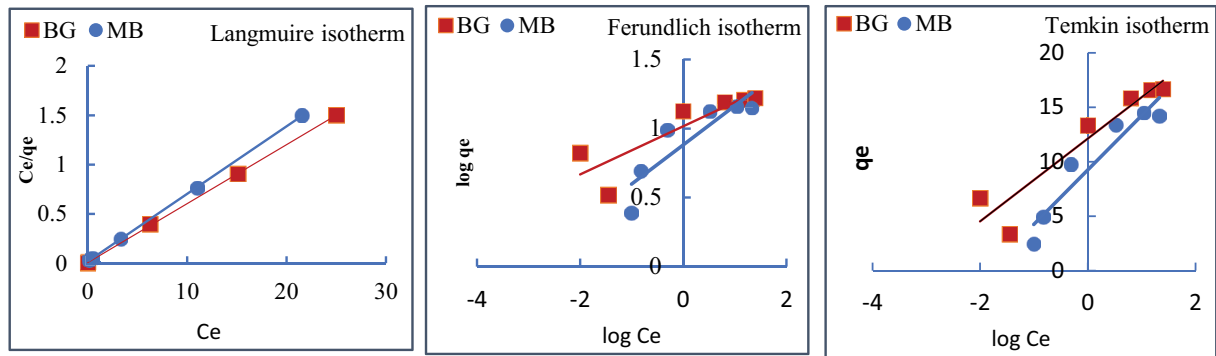

Fig. 11. Effect of temperature on removal dye (initial dye concentration: 5 mg/L; pH: 2; adsorbent dosage 35 g/L; contact time: 24 h)

Table 2
Thermodynamic parameters for the adsorption of MB and BG dye molecule onto the adsorbent

Dye	ΔS (J/mol·K)	T (K)	ΔG (kJ/mol)	ΔH (kJ/mol)
MB	+240.25	283	–1.45	+67.81
		298	–2.33	
		308	–7.26	
		318	–1.90	
BG	+487.6	283	–0.353	+140.54
		298	–2.849	
		308	–11.23	
		318	–0.0015	

Table 3
Parameters of the Langmuir and Freundlich and Temkin models for dye adsorption onto adsorbent

Dye	Langmuir		Freundlich		Temkin	
	Parameter	Value	Parameter	Value	Parameter	Value
MB [C = 20 mg/L; AD = 0.02 g/10 mL]	q_m	14.6 mg/g	$1/n$	0.2836	a_t	9.2444
	K_L	3.14	K_F	7.61	b_t	2.1645
	R^2	0.9998	R^2	0.7872	R^2	0.9055
	R_L	(0.0063–0.0598)				
BG [C = 20 mg/L; AD = 0.015 g/10 mL]	q_m	16.7 mg/g	$1/n$	0.1745	a_t	12.112
	K_L	7.29	K_F	10.38	b_t	1.6472
	R^2	0.9998	R^2	0.7579	R^2	0.8907
	R_L	(0.0027–0.0267)				

C: concentration; AD: adsorbent dose.

Fig. 12. Isotherm plots for adsorption of MB and BG on absorbent, Langmuir, Freundlich and Temkin isotherm model.

Table 4
Comparison of MB and BG adsorbent in different adsorbent materials

Adsorbents	Dyes	Adsorption capacity (mg/g)	References
Magnetic colloidal nanocrystal clusters (MCNCs) modified with 0.01 g poly(4-styrenesulfonic acid-co-maleic acid) sodium (PSSMA)	MB	7.81	[32]
Fe_3O_4/AC/CD/Alg polymer beads		2.079	[27]
Dry polymer beads		10.338	[27]
Superparamagnetic magnetite nanoparticles (Fe_3O_4 NPs)		10.47	[11]
Alginate grafted polyacrylonitrile beads		3.51	[33]
$CoFe_{1.9}Cr_{0.1}O_4$		11.41	[34]
Bis [Hg (2-Apt)]-Fe_3O_4 nanoparticles		14.6	This study
$Mn_{0.5}Cu_{0.5}Fe_2O_4$ nanospinels	BG	0.89	[35]
Salix alba leaves (SAL)		15.89	[36]
Tannin gel (TG)		20.41	[37]
Amine modified tannin gel (ATG)		8.55	[37]
Rambutan peels		9.64	[38]
Bis [Hg (2-Apt)]-Fe_3O_4 nanoparticles		16.7	This study
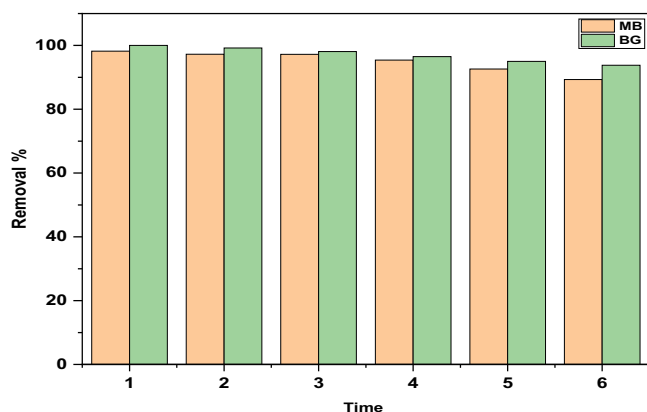
Fig. 13. Reusability of the Bis [Hg (2-Apt)]-Fe_3O_4 nanocomposites for MB and BG dye removal %.

desorbing solution, because of its economic and eco-friendly. After each desorption test, the reusability experiments were conducted in 6 cycles. Results indicated with each adsorption–desorption cycle, the removal efficiency for MB dye decreased gradually and stayed at 89.3% after the 6 cycles. In contrast, removal efficiency for BG dye was only marginally reduced and maintained at 93.8% after the 6 cycles (Fig. 13). Results suggested Bis [Hg (2-Apt)]-Fe_3O_4 nanocomposite can be used as an effective adsorbent for dye removal because of its excellent desorption and reuse capability.

3.9. Comparison with other adsorbents

Table 4 illustrates the adsorption capacity of MB and BG was considerable, compared to other adsorbents found in the literature.

4. Conclusions

The low-cost magnetic Fe_3O_4 nanoparticles coated on Bis [Hg (2-Apt)] were synthesized, evaluated, and used to remove the MB and BG dyes from the aqueous solution. The

water. Results showed that distilled water and ethanol are the best desorbing solution for both dyes, with the difference that the time required for distilled water was longer than for ethanol. However, distilled water was selected as a

findings showed that the highest removal efficiency of MB and BG was obtained at 97.55% and 100% at optimal conditions (adsorbent dose = 0.02 g/10 mL and 0.015 g/10 mL, pH = 5, initial dye concentration = 20 mg/L, and contact time = 120 and 70 min) respectively. The kinetic models exhibited that the MB (R^2 = 0.9995) and BG (R^2 = 1.0) adsorption process followed pseudo-second-order kinetics models and the adsorption was controlled by chemisorption process. Also, the Langmuir isotherm model indicated a better fit with experimental data than other isotherms. The maximum adsorption capacity (q_{max}) was obtained 14.6 and 16.7 mg/g for MB and BG respectively. The thermodynamics analysis showed that MB and BG adsorption onto the surface of the adsorbent was spontaneous, endothermic, and chemisorption. As a result, Bis [Hg (2-Apt)]-Fe$_3$O$_4$ nanocomposite could be considered an effective cationic dye adsorbent with excellent removal efficiency, regeneration, and reuse ability.

References

[1]   W. Li, Z. Xie, S. Xue, H. Ye, M. Liu, W. Shi, Y. Liu, Studies on the adsorption of dyes, Methylene blue, Safranin T, and Malachite green onto polystyrene foam, Sep. Purif. Technol., 276 (2021) 119435, doi: 10.1016/j.seppur.2021.119435.

[2]   V.S. Achari, R.M. Lopez, A.S. Rajalakshmi, S. Jayasree, O.M. Shibin, D. John, V. Sekkar, Microporous carbon with highly dispersed nano-lanthanum oxide (La$_2$O$_3$) for enhanced adsorption of Methylene blue, Sep. Purif. Technol., 279 (2021) 119626, doi: 10.1016/j.seppur.2021.119626.

[3]   N. Marzban, A. Moheb, S. Filonenko, S.H. Hosseini, M.J. Nouri, J.A. Libra, G. Farru, Intelligent modeling and experimental study on Methylene blue adsorption by sodium alginate-kaolin beads, Int. J. Biol. Macromol., 186 (2021) 79–91.

[4]   E.N. Heybet, V. Ugraskan, B. Isik, O. Yazici, Adsorption of Methylene blue dye on sodium alginate/polypyrrole nanotube composites, Int. J. Biol. Macromol., 193 (2021) 88–99.

[5]   I. Amar, A. Sharif, M. Ali, S. Alshareef, F. Altohami, M. Abdulqadir, M.M. Ahwidi, Removal of Methylene blue from aqueous solutions using nano-magnetic adsorbent based on zinc-doped cobalt ferrite, Chem. Method., 4 (2020) 1–18.

[6]   A. Ahmed, A. Ali, M. Ahmed, K.N. Parida, M. Ahmad, A. Ahmad, Construction and topological studies of a three dimensional (3D) coordination polymer showing selective adsorption of aromatic hazardous dyes, Sep. Purif. Technol., 265 (2021) 118482, doi: 10.1016/j.seppur.2021.118482.

[7]   M. Hassan, A.K. Deb, F. Qi, Y. Liu, J. Du, A .Fahy, M.A. Ahsan, S.J. Parikh, R. Naidu, Magnetically separable mesoporous alginate polymer beads assist adequate removal of aqueous Methylene blue over broad solution pH, J. Cleaner Prod., 319 (2021) 128694, doi: 10.1016/j.jclepro.2021.128694.

[8]   Z. Rezayati Zad, B. Moosavi, A. Taheri, Synthesis of monodisperse magnetic hydroxyapatite/Fe$_3$O$_4$ nanospheres for removal of Brilliant green (BG) and Coomassie Brilliant Blue (CBB) in the single and binary systems, Adv. J. Chem. B, 2 (2020) 159–171.

[9]   A. Samimi, Risk management in information technology, Prog. Chem. Biochem. Res., (2020) 130–134.

[10] J. Cheng, C. Zhan, J. Wu, Z. Cui, J. Si, Q. Wang, X. Peng, L.-S. Turng, Highly efficient removal of Methylene blue dye from an aqueous solution using cellulose acetate nanofibrous membranes modified by polydopamine, ACS Omega, 5 (2020) 5389–5400.

[11] A. Ramesh, D. Rama Devi, S. Mohan Botsa, K. Basavaiah, Facile green synthesis of Fe$_3$O$_4$ nanoparticles using aqueous leaf extract of *Zanthoxylum armatum* DC for efficient adsorption of Methylene blue, J. Asian Ceram. Soc., 6 (2018) 145–155.

[12] K. Sravanthi, D. Ayodhya, P.Y. Swamy, Green synthesis, characterization and catalytic activity of 4-nitrophenol reduction and formation of benzimidazoles using bentonite

[13] B.M.H. Ameen, H.A. Mohamad, Synthesis and characterization of Pd(II) and Pt(II) complexes with Bis [Hg (2-Apt)] compound, Kirkuk Univ. J. Sci. Stud., 13 (2018) 12–22.

[14] Y. Ji, C. Ma, J. Li, H. Zhao, Q. Chen, M. Li, H. Liu, A magnetic adsorbent for the removal of cationic dyes from wastewater, Nanomaterials, 8 (2018) 710, doi: 10.3390/nano8090710.

[15] Y. He, P. Wu, W. Xiao, G. Li, J. Yi, Y. He, C. Chen, P. Ding, Y. Duan, Efficient removal of Pb(II) from aqueous solution by a novel ion imprinted magnetic biosorbent: adsorption kinetics and mechanisms, PLoS One, 14 (2019) e0213377, doi: 10.1371/journal.pone.0213377.

[16] R.A. Sobh, H. Nasr, W.S. Mohamed, Synthesis and characterization of magnetic sponge nanocomposite for cleaning archeological lime stones, Egypt. J. Chem., 63 (2020) 507–514.

[17] S. Ahmadi, M. Fazilati, S.M. Mousavi, H. Nazem, Anti-bacterial/fungal and anti-cancer performance of green synthesized Ag nanoparticles using summer savory extract, J. Exp. Nanosci., 15 (2020) 363–380.

[18] S. Amutha, S. Sridhar, Green synthesis of magnetic iron oxide nanoparticle using leaves of *Glycosmis mauritiana* and their antibacterial activity against human pathogens, J. Innov. Pharm. Biol. Sci., 5 (2018) 22–26.

[19] S. Ahmadi, M. Fazilati, H. Nazem, S.M. Mousavi, Green synthesis of magnetic nanoparticles using *Satureja hortensis* essential oil toward superior antibacterial/fungal and anticancer performance, Biomed. Res. Int., 2021 (2021) 8822645, doi: 10.1155/2021/8822645.

[20] Y.P. Yew, K. Shameli, M. Miyake, N. Kuwano, N.B.B.A. Khairudin, S.E.B. Mohamad, K.X. Lee, Green synthesis of magnetite (Fe$_3$O$_4$) nanoparticles using seaweed (*Kappaphycus alvarezii*) extract, Nanoscale Res. Lett., 11 (2016) 1–7.

[21] G. Zhen, B.W. Muir, B.A. Moffat, P. Harbour, K.S. Murray, B. Moubaraki, K. Suzuki, I. Madsen, N. Agron-Olshina, L. Waddington, Comparative study of the magnetic behavior of spherical and cubic superparamagnetic iron oxide nanoparticles, J. Phys. Chem., 115 (2011) 327–334.

[22] A.R. Deshmukh, A. Gupta, B.S. Kim, Ultrasound assisted green synthesis of silver and iron oxide nanoparticles using fenugreek seed extract and their enhanced antibacterial and antioxidant activities, Biomed Res. Int., 2019 (2019) 1714358, doi: 10.1155/2019/1714358.

[23] N. Laskar, U. Kumar, Removal of Brilliant green dye from water by modified *Bambusa tulda*: adsorption isotherm, kinetics and thermodynamics study, Int. J. Environ. Sci. Technol., 16 (2019) 1649–1662.

[24] J. Chen, H. Chen, Removal of anionic dyes from an aqueous solution by a magnetic cationic adsorbent modified with DMDAAC, New J. Chem., 42 (2018) 7262–7271.

[25] N. Besharati, N. Alizadeh, S. Shariati, Removal of cationic dye Methylene blue (MB) from aqueous solution by coffee and peanut husk modified with magnetite iron oxide nanoparticles, J. Mex. Chem. Soc., 62 (2018) 110–124.

[26] N. Kataria, V. Garg, Application of EDTA modified Fe$_3$O$_4$/sawdust carbon nanocomposites to ameliorate Methylene blue and Brilliant green dye laden water, Environ. Res., 172 (2019) 43–54.

[27] S. Yadav, A. Asthana, R. Chakraborty, B. Jain, A.K. Singh, S.A. Carabineiro, M. Susan, A.B. Hassan, Cationic dye removal using novel magnetic/activated charcoal/β-cyclodextrin/alginate polymer nanocomposite, Nanomaterials, 10 (2020) 170, doi: 10.3390/nano10010170.

[28] J. Qiao, S. Gao, J. Yao, L. Zhang, N. Li, A rapid and green method for the removal of anionic dyes from aqueous solution using sulfobetaine-modified magnetic nanoparticles, AIP Adv., 9 (2019) 065308, doi: 10.1063/1.5101013.

[29] J. Saini, V. Garg, R. Gupta, Removal of Methylene blue from aqueous solution by Fe$_3$O$_4$@Ag/SiO$_2$ nanospheres: synthesis, characterization and adsorption performance, J. Mol. Liq., 250 (2018) 413–422.

[30] L. Liu, Z.Y. Gao, X.P. Su, X. Chen, L. Jiang, J.M. Yao, Adsorption removal of dyes from single and binary solutions using a

cellulose-based bioadsorbent, ACS Sustainable Chem. Eng., 3 (2015) 432–442.

[31] D. Zhang, M.-y. Zhu, J.-g. Yu, H.-w. Meng, F.-p. Jiao, Effective removal of Brilliant green from aqueous solution with magnetic Fe_3O_4@SDBS@LDHs composites, Trans. Nonferrous Met. Soc. China, 27 (2017) 2673–2681.

[32] Y.-B. Song, S.-N. Lv, C.-J. Cheng, G.-L. Ni, X.-W. Xie, W. Huang, Z.-G. Zhao, Fast and highly-efficient removal of Methylene blue from aqueous solution by poly (styrenesulfonic acid-co-maleic acid)-sodium-modified magnetic colloidal nanocrystal clusters, Appl. Surf. Sci., 324 (2015) 854–863.

[33] S. Ahmed, M.S. Mohd, A.N. Ahmedy, J.K. Khairil, Removal of Methylene blue dye from aqueous solution using alginate grafted polyacrylonitrile beads, Der Pharma Chem., 7 (2015) 237–242.

[34] I.A. Amar, A. Sharif, N.A. Omer, N.E. Akale, F. Altohami, M.A. Abdul Qadir, Synthesis and Characterization of Magnetic $CoFe_{1.9}Cr_{0.1}O_4$ Nanoparticles by Sol-Gel Method and Their

Applications as an Adsorbent for Water Treatment, First Conference for Engineering Sciences and Technology, 2018.

[35] S. Hashemian, A. Dehghanpor, M. Moghahed, $Cu_{0.5}Mn_{0.5}Fe_2O_4$ nano spinels as potential sorbent for adsorption of Brilliant green, J. Ind. Eng. Chem., 24 (2015) 308–314.

[36] R. Fiaz, M. Hafeez, R. Mahmood, Removal of Brilliant green (BG) from aqueous solution by using low cost biomass *Salix alba* leaves (SAL): thermodynamic and kinetic studies, J. Water Reuse Desal., 10 (2020) 70–81.

[37] N. Akter, M.A. Hossain, M.J. Hassan, M. Amin, M. Elias, M.M. Rahman, A.M. Asiri, I.A. Siddiquey, M.A. Hasnat, Amine modified tannin gel for adsorptive removal of Brilliant green dye, J. Environ. Chem. Eng., 4 (2016) 1231–1241.

[38] N.M. Nor, T. Hadibarata, Z. Yusop, Z.M. Lazim, Removal of Brilliant green and procionred dyes from aqueous solution by adsorption using selected agricultural wastes, J. Teknol., 74 (2015), doi: 10.11113/jt.v74.4880.
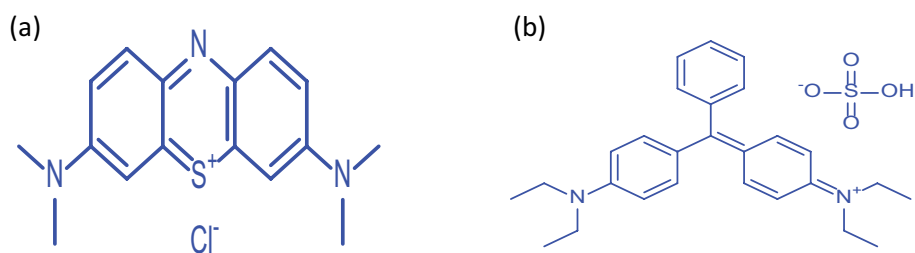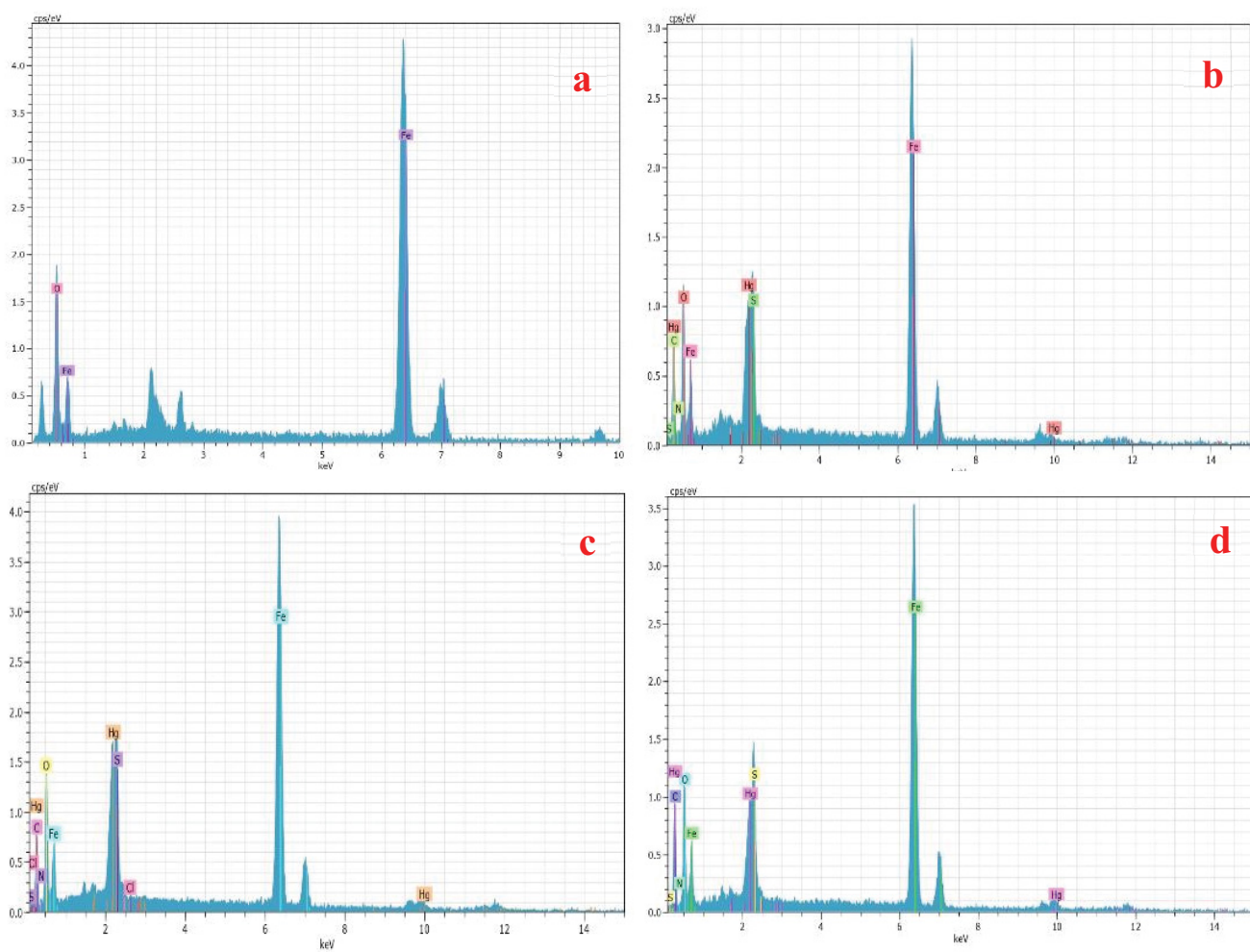
Supporting information

Fig. S1. Chemical structure of (a) MB, and (b) BG.

Fig. S2. EDX spectrum of the (a) Fe_3O_4, (b) Bis [Hg (2-Apt)]-Fe_3O_4, (c) Bis [Hg (2-Apt)]-Fe_3O_4 nanoparticles after adsorption of MB, and (d) Bis [Hg (2-Apt)]-Fe_3O_4 nanoparticles after adsorption of BG.